Alterations in Mitochondria-Associated Endoplasmic Reticulum Membranes Under Oxidative Stress in R28 Cells

Yuting Yang
Eye & ENT Hospital of Fudan University
Jihong Wu
Eye & ENT Hospital of Fudan University
Wei Lu
Eye & ENT Hospital of Fudan University
Yiqin Dai
Eye & ENT Hospital of Fudan University
Youjia Zhang
Eye & ENT Hospital of Fudan University
Xinghuai Sun (xhsun@shmu.edu.cn)
Eye & ENT Hospital of Fudan University

Research Article

Keywords: Mitofusin-2, hydrogen peroxide, hypoxia, Mitochondria-associated ER membranes, retinal precursor cells

Posted Date: March 21st, 2022

DOI: https://doi.org/10.21203/rs.3.rs-1432798/v1

Abstract

This study aimed to investigate alterations in mitochondria-associated endoplasmic reticulum membranes (MAMs) under oxidative stress conditions in R28 retinal precursor cells. Hydrogen peroxide (H_2O_2) and hypoxia (0.2% oxygen) were used to induce oxidative stress in R28 cells. Cell viability, reactive oxygen species (ROS) levels, mitochondrial membrane potential, mitochondrial calcium concentration, MAMs, and autophagy were evaluated. Mitofusin-2 (MFN2), a protein that plays a role in the structural regulation of MAMs, was either upregulated or downregulated in R28 cells to further explore the potential role of MFN2 in modulating MAMs. Oxidative stress not only modulated MAMs but also induced mitochondrial membrane potential (MMP) and increased mitochondrial calcium concentration. H_2O_2 and hypoxia also induced oxidative stress-associated autophagy in R28 cells. Additionally, autophagy inhibition increased MAM signaling. MFN2 silencing increased MAM expression and induced MMP collapse under normal conditions, whereas MFN2 upregulation rescued hypoxia-induced MAM alterations and alleviated MMP collapse. However, Mfn2 overexpression further enhanced H_2O_2-induced MAMs and failed to rescue MMP collapse. Our study indicates that MAMs possibly serve as a membrane source for oxidative stress-associated autophagy in R28 cells. MFN2 appears to play a negative role in maintaining MAM biogenesis under hypoxic conditions; however, its role in H_2O_2-associated MAM dysfunction remains unclear.

Introduction

Glaucoma is the most frequent cause of irreversible blindness worldwide and is characterized by progressive retinal ganglion cell dysfunction and visual field defects(Jonas et al. 2017). Reactive oxygen species (ROS) are biologically active free radicals that participate in a variety of cellular, physiological, and pathological processes. Oxidative stress usually results from either the excessive production or accumulation of intracellular ROS or both. Elevated intraocular pressure (IOP) and relative hypoxia in the retina stimulate ROS production, which in turn puts the retina and optic nerve under chronic stress, ultimately leading to progressive loss of RGCs, retinal and optic glial cell dysfunction, and ocular hemodynamic dysregulation(Nita and Grzybowski 2016).

Despite numerous studies on the relationship between oxidative stress and RGC death in the past decade(Tezel et al. 2007), the prognosis of glaucoma remains low. Therefore, exploring new therapeutic strategies for oxidative neuronal degeneration and elucidating the molecular pathways underlying RGC death will provide insights into future therapeutics for retinal degeneration.

Mitochondria-associated ER membranes (MAMs) are the region of the ER that connects it to the mitochondria and serves as the location of many chaperone proteins that regulate cell homeostasis, including autophagy (Park et al. 2017; Giacomello and Pellegrini 2016; Rowland and Voeltz 2012; Yuan et al. 2020; Manganelli et al. 2020). Multiple factors, such as mitofusin-2 (MFN2), contribute to the maintenance of a relatively stable MAM structure(Paillusson et al. 2016). Previous studies have reported a controversial role of MFN2 in MAM biogenesis(Hu et al. 2021; de Brito and Scorrano 2008; Naon et al.

2016); however, only a few have explored its role in oxidative damage-associated MAM alterations in retinal cells. Additionally, studies on the roles of MAMs in glaucoma have mostly focused on the role of the Sigma 1 receptor in RGC protection, and not on the structural and functional changes of MAMs during this process.

This study aimed to explore the alterations in MAMs in the pathogenesis of oxidative damage in retinal cells and the potential role of MFN2 in modulating MAM homeostasis in R28 cells.

Material And Methods

Antibodies:

The following commercial antibodies (vendor, catalog number) were used for western blot analyses and immunofluorescence staining according to manufacturers' instructions: mouse anti-LC3B(E5Q2K) antibody (Cell Signaling Technology, 83506), rabbit anti-p62,SQSTM1 polyclonal antibody (Proteintech, 18420-1-AP), rabbit anti-MFN2 polyclonal antibody (Proteintech, 12186-1-AP), mouse anti-VDAC1/Porin antibody [20B12AF2] (Abcam, ab14734), rabbit anti-ITPR3 polyclonal antibody (Thermo Fisher Scientific, PA5-79544), mouse anti-beta Actin monoclonal antibody HRP (Proteintech, HRP-66009), anti-rabbit IgG, HRP-linked Antibody (Cell Signaling Technology, 7074), anti-mouse IgG, HRP-linked Antibody (Cell Signaling Technology, 7076), and donkey anti-rabbit IgG (H + L) highly cross-adsorbed secondary antibody Alexa Fluor 594 (Thermo Fisher Scientific, A21207).

Plasmids

Mfn2 cDNA was purchased from Hanbio (Shanghai) and cloned into expression vector with 3flag tag, and MFN2 protein expression plasmid was constructed.

Primers:

PC-r-*Mfn2*-E-B-F, 5'-AGACCCAAGCTGGCTAGTTGAATTCGCCACCATGTCCCTGCTCTTTTCT-3';

PC-r-*Mfn2*-E-B-R, 5'- TCACTTAAGCTTGGTACCGAGGATCCTCTGCTGGGCTGCAGGTACTGGT – 3'

shRNA

Mfn2 shRNAs, and nonsense control shRNAs, which were inserted to plasmid vector, were purchased from Hanbio Shanghai.

The shRNA target sequences used in this study are:

non-sense, 5'- TTCTCCGAACGTGTCACGTAA – 3';

Mfn2 1, 5'- CAGAAGAGCAGGTCCTGGATGTCAA-3';

Mfn2 2, 5'- CGGAGCTGGACAGCTGGATTGATAA – 3';

Mfn2 3, 5'- GAGGAGCTCATGGTCTCCATGGTTA – 3';

Cell culture

The R28 retinal precursor cell line was generously offered by Dr. Guotong Xu (Tongji Eye Institute, Tongji University School of Medicine, Shanghai, China) and cultured in low glucose Dulbecco's modified Eagle's medium (Sigma-Aldrich, USA) with 10% Fetal Bovine Serum (Thermo Fisher Scientific, USA), 100 U/ml penicillin and 100 mg/ml streptomycin (Thermo Fisher Scientific, USA) in a 37°C humidified atmosphere containing 5% CO_2.

Cell viability assay (CCK-8)

Cell viability was measured with Cell Counting Kit-8 (CCK-8) (Beyotime Biotechnology, China) as the protocol described. Briefly, R28 cells were plated in 96-well plates and incubated with H_2O_2 or other treatments. After treatments, cells were washed with PBS for twice and fresh medium with 10% CCK-8 reagent were added, the absorbance of the assay plates was measured at 450 nm following 2-hour incubation.

Transient transfection:

Transient transfection was applied to develop Mfn2-overexpression or Mfn2-knockdown R28 cells. Gfp (Green Fluorescent Protein, used as control) coding plasmid (1000ng/ml), and Mfn2 coding plasmid (500ng/ml), control shRNA (1000ng/ml) and Mfn2 shRNA (250ng/ml) provided by Hanbio (Shanghai) were transfected with Lipo2000 (Thermo Fisher Scientific, USA) in no serum Opti-MEM (Thermo Fisher Scientific, USA) according to manufactory instruction.

Proximity ligation assay (PLA)

PLA was conducted according to manufactory instructions (DUOLINK®, Sigma-Aldrich, France). Firstly, specific antibodies were used to label the targeted components. Then, secondary antibodies conjugated with oligonucleotides (PLA probe MINUS and PLUS) were added to the reaction and incubated. Additionally, the Ligation solution, consisting of two oligonucleotides and Ligase, was added and the oligonucleotides would hybridize to the two PLA probes and joined to a closed circle if they were in proximity (< 30nm). What's more, the Amplification solution, consisting of nucleotides and fluorescently labeled oligonucleotides, was added together with Polymerase. The oligonucleotide arm of one of the PLA probes acted as a primer for a rolling-circle amplification (RCA) reaction using the ligated circle as a template, generated a concatemeric (repeated sequence) product. The fluorescently labeled oligonucleotides would hybridize to the RCA product. The signal was easily visible as a distinct fluorescent spot and analyzed by confocal microscopy (Leica, Germany). A minimum of 9 images were taken per sample, and three independent series were performed for each treatment.

JC-1 assay

JC-1 kit (Beyotime Biotechnology, China) was used to detect mitochondrial membrane potential. Briefly, after H_2O_2 treatment, cells were rinsed with 1x washing buffer once and then incubated with JC-1 reagent

for 20 minutes at 37 ℃. Cells were then washed with 1x washing buffer three times and read at 488/525 nm (monomers) and 550/590 nm (aggregates).

Rhod-2 staining

Rhod-2 dye was provided by AAT Bioquest (Canada) and used to measure mitochondrial calcium. R28 cells were plated on black 96-well plates. 100 µl 2x Rhod-2 dye was added into desired wells containing 100µl culture medium and incubated in the cell incubator for 30 minutes. The dye working solution was replaced with HHBS and cells were treated with H_2O_2 for the indicated time.

ROS Assay

Quantitation of intracellular reactive oxygen species (ROS) accumulation was performed by fluorescence detection using the fluorescent probe 2_,7_-dichlorofluorescein diacetate (DCFH-DA), (Beyotime Biotechnology, China). R28 cells were subjected to the appropriate treatments and then incubated for 20 minutes in the dark at 37 ℃ with 10 µM DCFH-DA solutions. After incubation, the cells were analyzed within 30 min. Mean fluorescence intensity of ROS was measured using a fluorescence microscope.

Mito-tacker and ER-tracker staining and Quantitative Colocalization Analysis

After H_2O_2 treatments, R28 cells were loaded with 500 nM MitoTracker Red FM (Invitrogen, USA) and 1000 nM ER-Tracker Blue-White DPX (Invitrogen, USA) at 37°C for 30 minutes. R28 cells were then quickly rinsed with warm DPBS once (Sigma-Aldrich, USA) and then fixed with 4% PFA for 5 minutes at room temperature. Images were captured with confocal microscopy with a 60x oil immersion objective and processed using NIH's Image J software. Colocalization of the ER and mitochondria was calculated as Manders' Colocalization Coefficient (MCC) using JACoP plugin in 5 randomly selected images per condition in each independent experiment. Auto-thresholds were applied for both channels to select pixels for colocalization analysis.

Fluorescent microscopy and image analyses

R28 cells were quickly rinsed with cold DPBS once (Sigma-Aldrich, USA) and then fixed with 4% PFA for 10 minutes at room temperature. Cells were permeabilized with 0.4% Triton X-100 (Sigma-Aldrich, USA) in DPBS for 15 minutes at room temperature and then incubated with blocking buffer (1x DPBS with 0.1% Triton X-100 and 5% BSA) for 30 minutes. R28 cells were stained with primary antibodies overnight at 4°C and rinsed three times with 1x DPBS. Cells were then incubated with Alexa Fluor secondary antibodies for 1 hour at room temperature, rinsed three times with 1x DPBS, mounted with VECTASHIELD Antifade Mounting Medium with DAPI (Vector Laboratories H-1200, USA) or Antifade Mounting Medium without DAPI (Beyotime Biotechnology, China), and stored at 4 ℃ until imaging.

Western blot analyses

R28 cell lysates were prepared by incubating cells with ice-cold 1x lysis buffer (Beyotime Biotechnology, China), cOmplete proteinase inhibitor cocktail (Roche, Switzerland) and Phosphatase Inhibitor Cocktail

(Roche, Switzerland) on ice for 20 minutes. Cell lysates were then centrifuged at 12,000 g at 4℃ for 15 minutes to remove the insoluble fractions. The supernatant was then mixed with 5x sample loading buffer (Beyotime Biotechnology, China) and boiled for 7 minutes. Denatured proteins were separated by SDS-PAGE using 4–20% SurePAGE, Bis-Tris precast protein gels (GenScript, China) and transferred to Immun-Blot PVDF membranes (Millipore). Membranes were blocked with 5% non-fat milk or 5% BSA in 1x TBS buffer containing 0.05% Tween 20 (TBST), incubated with primary and secondary antibodies diluted according to manufacturers' instructions, and washed five times with 1x TBST. Protein bands were visualized with Immobilon Western Chemilum HRP Substrate (Millipore, USA) on a BioSpectrum imaging system (Ultra-Violet Products, China).

Statistical analyses

Quantitative data were expressed as mean (± SD). Unpaired Student's t-test was performed when comparing two groups and one-way ANOVA test for three groups and more. Statistical differences were considered significant when P value is less than 0.05.

Results

Oxidative Stress Induces Mitochondrial Dysfunction in R28 Cells

Hydrogen peroxide (H_2O_2) is a small molecule that can pass freely through the cell membrane and induce oxidative stress. Therefore, we used this molecule as an oxidative stress inducer in our study. In addition, we exposed the cells to 0.2% O_2 which is a relatively moderate oxidative inducer. Details regarding the concentration and timepoints for either condition are available in **Supplementary Fig. S1 and S2**.

We assessed mitochondrial homeostasis, including mitochondrial calcium concentration and membrane potential, following H_2O_2 (400 μM) treatment and hypoxia (0.2% O_2, 2 days) induction.

Rhod-2 staining (5 μM) was used to detect mitochondrial calcium concentration, and the results indicated that H_2O_2 induced a mitochondrial calcium spark as early as 10 min, which reached a peak at 45 min (Fig. 1a). Similarly, hypoxia (0.2% O_2, 2 days) also induced mitochondrial calcium sparks in R28 cells (Fig. 1c).

Additionally, the JC-1 assay was used to detect the changes in mitochondrial membrane potential. Red signals indicate mitochondrial aggregates (due to high mitochondrial membrane potential), while green signals indicate monomers (due to low mitochondrial membrane potential). Upon exposing R28 cells to H_2O_2 (400 μM) or hypoxic condition, the red signal was reduced, the green signal was increased, and the green-to-red ratio was significantly elevated **(**Fig. 1b, 1d**).** These results suggested that oxidative stress-induced by H_2O_2 or hypoxia causes mitochondrial dysfunction in a time-dependent manner.

Oxidative Stress Increases MAMs in R28 Cells

Next, we detected alterations in MAMs in R28 cells under normal and oxidative stress conditions. First, we co-stained R28 cells with a mitochondria-specific dye (MitoTracker) and an ER-specific dye (ER-tracker). Images were obtained with a Leica confocal microscope, and Mander's coefficients were calculated using ImageJ software. Both H_2O_2 (400 μM) and hypoxia (0.2% O_2) treatments increased the colocalization of mitochondria and ER in a time-dependent manner (Fig. 2a-d). Given the limitations of light microscopy, we further applied the proximity ligation assay (PLA) to detect the coupling between mitochondrial VDAC1 and ER ITPR3, in which signals could be detected only if the distance between the mitochondria and ER was < 30 nm. The PLA signal alterations were consistent with the colocalization analyses, indicating that oxidative stress increased MAMs in R28 cells. Furthermore, autophagy inhibition with bafilomycin A1 (100 nM, 1 h), a late-stage autophagy inhibitor further increased the colocalization between the mitochondria and ER (Fig. 2e-g).

MAMs Serve as a Membrane Source for Oxidative Stress-Induced Autophagy

Autophagy is a highly conserved process that plays a dual role in regulating the survival and death of retinal cells. (Lin and Kuang 2014) Immunofluorescence assay showed that H_2O_2 and hypoxia resulted in accumulation of LC3 puncta in R28 cells (Fig. 3a), which could be due to the induction of autophagy or inhibition of autophagosome turnover. We further performed western blotting to monitor both p62 degradation and LC3 turnover. Western blot analyses showed that p62 degradation and LC3 II conversion were increased after exposure to H_2O_2 (200 and 400 μM, 2 and 6 h) or hypoxic conditions (0.2% O_2 for 2 days) (Fig. 3b-g). Since the autophagy inhibitors enhanced PLA signals (Fig. 2e,2f), we speculated that MAMs serve as a membrane source for oxidative stress-associated autophagy.

Modulation of MFN2 Expression Levels Alters MAMs

Our western blot results showed that H_2O_2 and hypoxia decreased MFN2 expression levels (Fig. 4a-d); thus, we investigated whether Mfn2 overexpression could alleviate oxidative stress-induced MAM dysfunction. Therefore, *Mfn2* was upregulated or downregulated in R28 cells using transient transfection assays (Fig. 4e). Under normal conditions, *Mfn2* knockdown significantly increased the number of contact points between the mitochondria and ER, as evidenced by increased VDAC1/ITPR3 interactions compared to the control cells; however, there was no statistically significant difference between the *Mfn2*-overexpressing and the control groups (Fig. 4c, 4d). JC-1 assay also showed that *Mfn2* knockdown resulted in MMP collapse under normal conditions (Fig. 4e, 4f). Additionally, MFN2 overexpression in R28 cells rescued hypoxia-induced ER-mitochondria tether elevation, as evidenced by in situ PLA signals (Fig. 4g, 4h), and rescued MMP collapse in R28 cells (Fig. 4i, 4j). In contrast, *Mfn2* overexpression further enhanced H_2O_2-induced MAMs and failed to rescue MMP collapse. These results indicate that MFN2 plays a negative role in maintaining MAM biogenesis under hypoxic conditions; however, its role in H_2O_2 associated MAM dysfunction remains unclear.

Discussion

This study revealed the association between MAMs and oxidative stress–associated mitochondrial dysfunction. We showed that both H_2O_2 and hypoxia increased ER-mitochondrial tethers and induced mitochondrial dysfunction in R28 cells.

The role of MFN2 in modulating mitochondrial ER tethers is controversial. ER resident MFN2 assembles homodimer or heterodimer complexes with outer mitochondrial membrane–resident MFN2 and maintains Ca^{2+} transport. One study found that the abundance of MAMs and the extent of energy stress–induced autophagy are significantly attenuated in mouse embryonic fibroblasts lacking MFN2 (*mfn2*$^{-/-}$) (Hu et al. 2021). Controversially, another study claimed that Mfn2 knockdown promoted mitochondrial-ER tether and increased mitochondrial calcium levels.(Filadi et al. 2015) In our study, we showed that *Mfn2* overexpression reduced hypoxia-induced ER-mitochondrial tethers but exerted no effect on H_2O_2-induced MAM dysfunction, suggesting that MFN2 serves as a negative player in maintaining MAMs. In addition, MFN2 overexpression alleviated hypoxia-induced MMP collapse. This study is the first to connect MAM dysfunction to oxidative stress–associated retinal cell injury and identifies MFN2 as a therapeutic target for hypoxia-induced MAM dysfunction.

This study had some limitations. Although *Mfn2* overexpression rescued hypoxia-induced MAM dysfunction, we did not determine the underlying mechanism of this effect. Additionally, the change in the distance between the mitochondria and ER is an essential pathological change in neurodegenerative diseases, and co-staining of MitoTracker or ER-tracker with PLA failed to show the detailed structures of MAMs(Hedskog et al. 2013).

R28 retinal neuronal precursor cells were selected because they are immortalized and suitable for the measurement of multiple physiological and pathological processes. However, they may not behave similar to primary retinal cells. Therefore, it is necessary to reproduce this study in primary retinal cells, such as RGCs and amacrine cells, to better understand the effects of oxidative stress on retinal cells.

Declarations

ACKNOWLEDGMENTS

We thank Dr. Guotong Xu for generously providing the retinal precursor cell line.

Funding

This work was supported by the subject of major projects of National Natural Science Foundation of China (81790641) and the State Key Program of National Natural Science Foundation of China (82030027).

Competing Interests

The authors have no relevant financial or non-financial interests to disclose.

Author Contributions

All authors contributed to the study conception and design. Material preparation, and analysis were performed by Jihong Wu, Wei Lu and Yuting Yang. Jihong Wu and Yiqin Dai prepared supplementary figure 1-2. Wei Lu and Youjia Zhang prepared figure 1. Yuting Yang prepared figure 2-4. The first draft of the manuscript was written by Yuting Yang and Xinghuai Sun. Xinghuai Sun revised the manuscript. All authors read and approved the final manuscript.

References

1. de Brito, O. M., and L. Scorrano. 2008. 'Mitofusin 2 tethers endoplasmic reticulum to mitochondria', *Nature*, 456: 605-10.
2. Filadi, R., E. Greotti, G. Turacchio, A. Luini, T. Pozzan, and P. Pizzo. 2015. 'Mitofusin 2 ablation increases endoplasmic reticulum-mitochondria coupling', *Proc Natl Acad Sci U S A*, 112: E2174-81.
3. Giacomello, M., and L. Pellegrini. 2016. 'The coming of age of the mitochondria-ER contact: a matter of thickness', *Cell Death Differ*, 23: 1417-27.
4. Hedskog, L., C. M. Pinho, R. Filadi, A. Ronnback, L. Hertwig, B. Wiehager, P. Larssen, S. Gellhaar, A. Sandebring, M. Westerlund, C. Graff, B. Winblad, D. Galter, H. Behbahani, P. Pizzo, E. Glaser, and M. Ankarcrona. 2013. 'Modulation of the endoplasmic reticulum-mitochondria interface in Alzheimer's disease and related models', *Proc Natl Acad Sci U S A*, 110: 7916-21.
5. Hu, Y., H. Chen, L. Zhang, X. Lin, X. Li, H. Zhuang, H. Fan, T. Meng, Z. He, H. Huang, Q. Gong, D. Zhu, Y. Xu, P. He, L. Li, and D. Feng. 2021. 'The AMPK-MFN2 axis regulates MAM dynamics and autophagy induced by energy stresses', *Autophagy*, 17: 1142-56.
6. Jonas, J. B., T. Aung, R. R. Bourne, A. M. Bron, R. Ritch, and S. Panda-Jonas. 2017. 'Glaucoma', *Lancet*, 390: 2183-93.
7. Lin, W. J., and H. Y. Kuang. 2014. 'Oxidative stress induces autophagy in response to multiple noxious stimuli in retinal ganglion cells', *Autophagy*, 10: 1692-701.
8. Manganelli, V., P. Matarrese, M. Antonioli, L. Gambardella, T. Vescovo, C. Gretzmeier, A. Longo, A. Capozzi, S. Recalchi, G. Riitano, R. Misasi, J. Dengjel, W. Malorni, G. M. Fimia, M. Sorice, and T. Garofalo. 2020. 'Raft-like lipid microdomains drive autophagy initiation via AMBRA1-ERLIN1 molecular association within MAMs', *Autophagy*: 1-21.
9. Naon, D., M. Zaninello, M. Giacomello, T. Varanita, F. Grespi, S. Lakshminaranayan, A. Serafini, M. Semenzato, S. Herkenne, M. I. Hernandez-Alvarez, A. Zorzano, D. De Stefani, G. W. Dorn, and L. Scorrano. 2016. 'Critical reappraisal confirms that Mitofusin 2 is an endoplasmic reticulum-mitochondria tether', *Proceedings of the National Academy of Sciences of the United States of America*, 113: 11249-54.

10. Nita, M., and A. Grzybowski. 2016. 'The Role of the Reactive Oxygen Species and Oxidative Stress in the Pathomechanism of the Age-Related Ocular Diseases and Other Pathologies of the Anterior and Posterior Eye Segments in Adults', *Oxid Med Cell Longev*, 2016: 3164734.
11. Paillusson, S., R. Stoica, P. Gomez-Suaga, D. H. W. Lau, S. Mueller, T. Miller, and C. C. J. Miller. 2016. 'There's Something Wrong with my MAM; the ER-Mitochondria Axis and Neurodegenerative Diseases', *Trends Neurosci*, 39: 146-57.
12. Park, S. J., S. B. Lee, Y. Suh, S. J. Kim, N. Lee, J. H. Hong, C. Park, Y. Woo, K. Ishizuka, J. H. Kim, P. O. Berggren, A. Sawa, and S. K. Park. 2017. 'DISC1 Modulates Neuronal Stress Responses by Gate-Keeping ER-Mitochondria Ca(2+) Transfer through the MAM', *Cell Rep*, 21: 2748-59.
13. Rowland, A. A., and G. K. Voeltz. 2012. 'Endoplasmic reticulum-mitochondria contacts: function of the junction', *Nat Rev Mol Cell Biol*, 13: 607-25.
14. Tezel, G., X. Yang, C. Luo, Y. Peng, S. L. Sun, and D. Sun. 2007. 'Mechanisms of immune system activation in glaucoma: oxidative stress-stimulated antigen presentation by the retina and optic nerve head glia', *Invest Ophthalmol Vis Sci*, 48: 705-14.
15. Yuan, L., Q. Liu, Z. Wang, J. Hou, and P. Xu. 2020. 'EI24 tethers endoplasmic reticulum and mitochondria to regulate autophagy flux', *Cell Mol Life Sci*, 77: 1591-606.

Figures

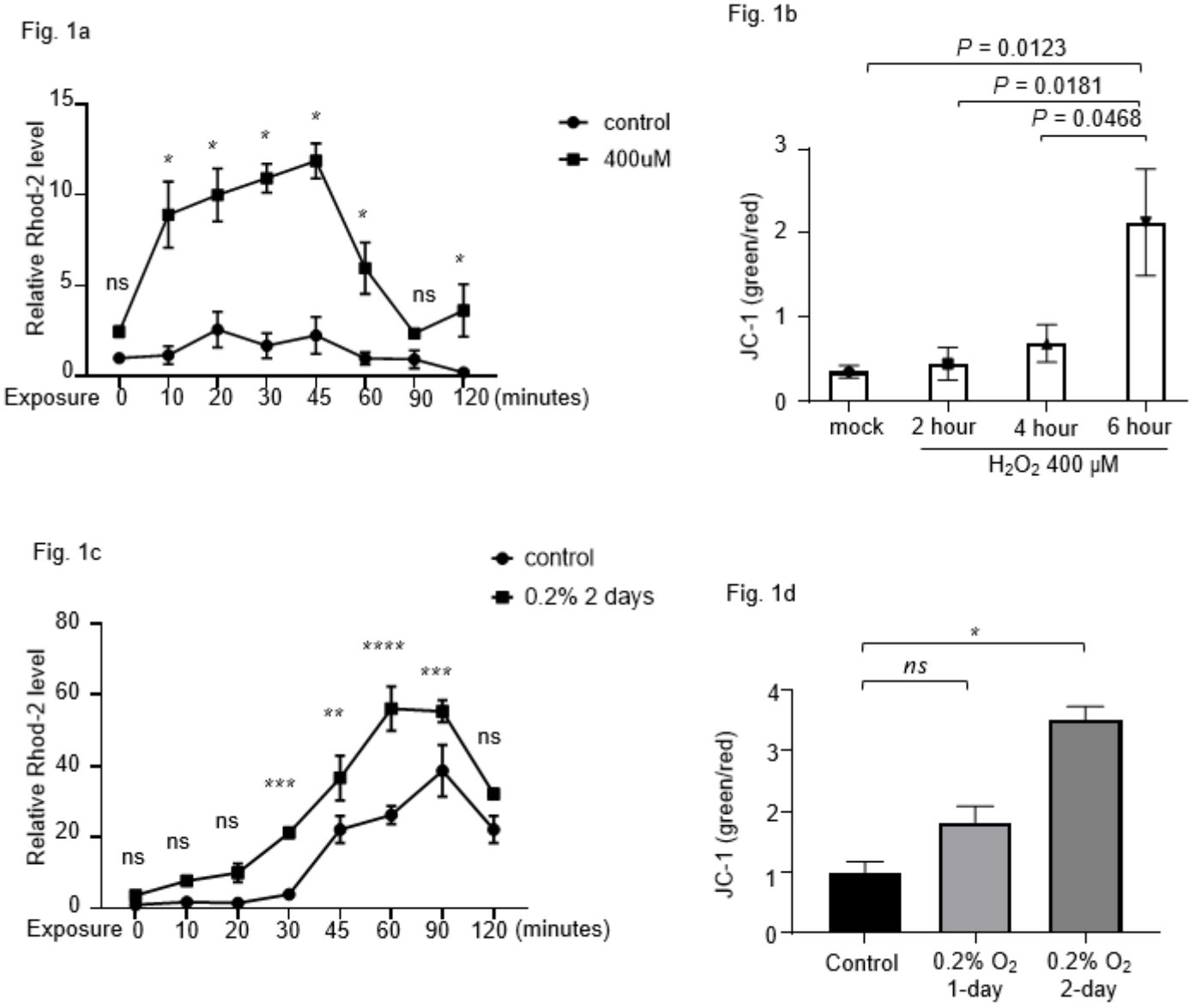

Figure 1

H_2O_2 and hypoxia induce mitochondrial dysfunction in R28 cells

a H_2O_2 increases mitochondrial calcium flux as early as 10 min, with the effect reaching a peak at 45 min in a time-dependent manner. **b** JC-1 assay showing H_2O_2 (400 μM) induced mitochondrial depolarization in R28 cells. **c** Hypoxic incubation (0.2% O_2) increased mitochondrial calcium flux as early as 30 min, reaching a peak at 60 min in a time-dependent manner. **d** JC-1 assay showing that hypoxia induces mitochondrial depolarization. Analysis of relative rhod-2 **(a, c)** and JC-1 fluorescence intensities **(b, d)** using ImageJ software. *P*-values were determined using a one-way analysis of variance with Tukey's test for multiple comparisons. * $p < 0.0001$.

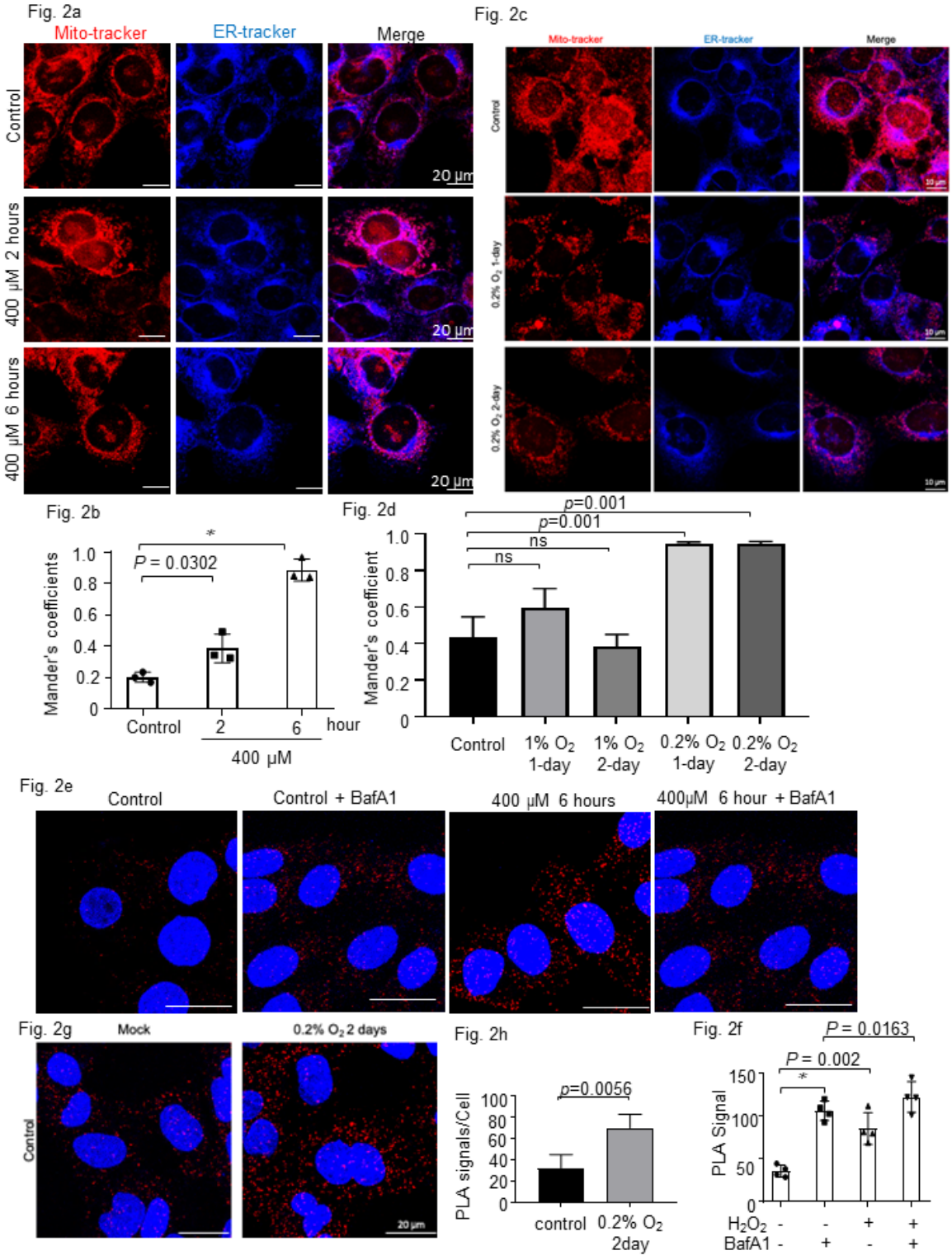

Figure 2

Oxidative stress increases ER-mitochondrial tethers in R28 cells

(a, c) R28 cells co-stained with MitoTracker and ER-Tracker. Scale bars, 10 mm. (**a, c)** H_2O_2 (400 μM) **(a)** and hypoxia (0.2% O_2) **(c)** increase the colocalization of mitochondria and ER. **(b, d)** Colocalization analyses calculated as Mander's coefficients (MCC) using ImageJ software, and *P*-values were

determined using a one-way analysis of variance with Dunnett's test for multiple comparisons. **(e, g)** PLA signals show that H_2O_2 (400 μM) **(e)** or hypoxia (0.2% O_2) **(f)** increase MAM signaling, as evidenced by the increased VDAC1/ITPR3 interactions in R28 cells in a time-dependent manner. PLA signals also show that bafilomycin A1 (100 nM, 1 h before fixation) further increases PLA signals under both normal and oxidative stress conditions **(e)**. Scale bars, 20 mm. **(h, f)** PLA signals (PLA puncta numbers per cell) were analyzed using ImageJ software, and *P*-values were determined using a one-way analysis of variance with Dunnett's test and a one-way analysis of variance with Tukey's test for multiple comparisons, respectively. * $p < 0.001$.

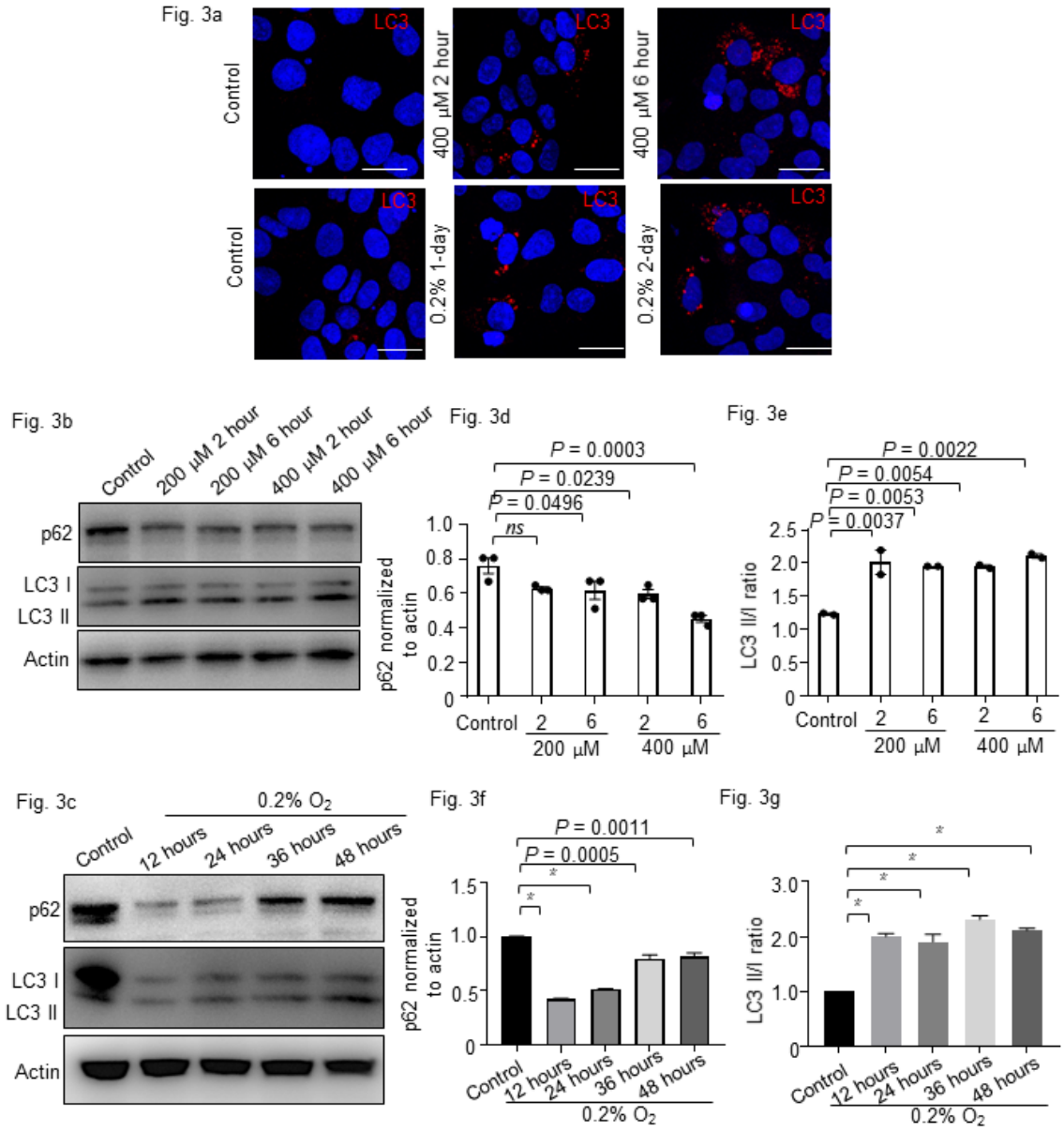

Figure 3

MAMs serve as a membrane source of ROS for oxidative stress–induced autophagy in R28 cells

a Representative fluorescent micrographs of LC3 puncta in R28 cells treated with H_2O_2 (400 μM, 2, or 6 h) or hypoxia (0.2% O_2). Scale bars, 20 mm. (**b, c)** R28 cells were either treated with H_2O_2 (200 and 400 μM) **(b)** or put under hypoxic conditions (0.2% O_2) **(c)** for the indicated time. Western blots of the indicated

proteins in whole-cell lysates are shown. The p62, LC3 II/I, and actin bands were analyzed via densitometry using the ImageJ software. **(d-g)** The ratios of p62/Actin and LC3 II/I were quantified. Bars in (**d-g)** represent the mean ± SD of three replicates. *P*-values were determined using a two-way analysis of variance with Sidak's multiple comparisons. * $p < 0.0001$.

Figure 4

Modulation of MFN2 expression levels alters MAMs and the mitochondrial membrane potential

(a, c) H_2O_2 (200, 400, and 800 μM) **(a)** or hypoxia (0.2% O_2) **(c)** were used to mimic oxidative stress conditions in R28 cells for the indicated time. MFN2 and actin protein levels were examined via western blotting. **(b, d)** MFN2 and actin bands were analyzed via densitometry using ImageJ software, and the ratio of MFN2/Actin was quantified. Representative fluorescent micrographs (**e**) and quantification (**f**) of PLA in control, Mfn2-overexpressing, and Mfn2-deficient R28 cells under normal, H_2O_2 (400 μM), or hypoxic (0.2% O_2) conditions. Scale bars, 20 mm. **(g)** Quantification of control, Mfn2-overexpressing, and Mfn2-deficient R28 cells under oxidative stress conditions (H_2O_2 or hypoxia) using JC-1 assays. Bars in **b, d, f, and g** represent the mean ± SD of four replicates. *P*-values were determined using a one-way analysis of variance with Tukey's test for multiple comparisons. * $p < 0.001$.

Supplementary Files

This is a list of supplementary files associated with this preprint. Click to download.

- supplementaryfigure.pptx
- SupplementaryFigurelegend.docx